

**This is an electronic reprint of the original article.
This reprint *may differ* from the original in pagination and typographic detail.**

Author(s): Lahti, Riikka; Bergna, Davide; Romar, Henrik; Hu, Tao; Comazzi, Alberto; Pirola, Carlo; Bianchi, Claudia L.; Lassi, Ulla

Title: Characterization of Cobalt Catalysts on Biomass-Derived Carbon Supports

Year: 2017

Version:

Please cite the original version:

Lahti, R., Bergna, D., Romar, H., Hu, T., Comazzi, A., Pirola, C., Bianchi, C. L., & Lassi, U. (2017). Characterization of Cobalt Catalysts on Biomass-Derived Carbon Supports. *Topics in Catalysis*, 60(17-18), 1415-1428. <https://doi.org/10.1007/s11244-017-0823-z>

All material supplied via JYX is protected by copyright and other intellectual property rights, and duplication or sale of all or part of any of the repository collections is not permitted, except that material may be duplicated by you for your research use or educational purposes in electronic or print form. You must obtain permission for any other use. Electronic or print copies may not be offered, whether for sale or otherwise to anyone who is not an authorised user.

Characterization of cobalt catalysts on biomass-derived carbon supports

Riikka Lahti^{1,2,*}, Davide Bergna^{1,2}, Henrik Romar^{1,2}, Tao Hu¹,

Alberto Comazzi³, Carlo Pirola³, Claudia L. Bianchi³, Ulla Lassi^{1,2}

¹ University of Oulu, Research Unit of Sustainable Chemistry, P.O.Box 3000, FI-90014 University of Oulu, Finland

² University of Jyväskylä, Kokkola University Consortium Chydenius, Applied Chemistry, P.O.Box 567, FI- 67101
Kokkola, Finland

³ Università degli Studi di Milano, Dipartimento di Chimica, Via Golgi, 19 - 20133 Milano, Italy

* *E-mail address:* riikka.lahti@chydenius.fi

Abstract

Cobalt catalysts are known to have a high activity and selectivity in the Fischer-Tropsch reaction converting synthesis gas to higher hydrocarbons (C₅₊). These catalysts have been supported by different porous materials. Porous carbon materials like activated carbon (AC) have physical and chemical surface properties that affect the preparation of supported metal catalysts and can easily be tailored.

In this study, AC was produced by carbonization and steam activation of lignin, a waste fraction from the Kraft pulping process. A series of Co/AC-catalysts was produced and characterized by several techniques.

According to the results, tailored properties (high surface area, mesoporosity) were obtained for carbon supports. Further, ash content could be reduced by acid treatment. Co/AC-catalysts prepared by ultrasonic assisted impregnation have high metal dispersion (10.1%). It was also observed that small metal particles were difficult to reduce, but acid (HNO₃) treatment has a positive effect on reduction temperatures.

Keywords: activated carbon, catalyst, characterization, cobalt, support

27 **1. Introduction**

28 The sustainable catalytic conversion of renewable resources to chemicals and fuels is a rapidly growing field
29 in research. Practically all fuels and over 85% of the chemicals coming out of petrochemical refineries have
30 seen at least one catalytic conversion step in their production process. Conventional catalysts have been
31 supported by a number of supports, such as Al_2O_3 , SiO_2 , and TiO_2 . Many recent reviews deal with the
32 advantages of carbon supports for the preparation of highly dispersed metal catalysts. Porous carbon
33 materials like activated carbon (AC) have physical and chemical surface properties that can easily be such as
34 a large surface area, the proper pore size distribution and acid-base characters on the surface that affect to
35 the preparation of metal supported catalysts.[1-3]

36 Cobalt-based catalysts are known to have a high activity in the Fischer-Tropsch reaction (FT) converting
37 synthesis gas into linear hydrocarbons and waxes and have low activity for the water gas shift reaction. Many
38 studies have been done with different preparation methods, cobalt loading, and supports.[4-9] It has been
39 found that the support materials have a significant role on the activity of the heterogeneous catalysts.
40 However, a strong metal-support interaction between cobalt and conventional oxide supports (Al_2O_3 , SiO_2 ,
41 etc.) inhibits the formation of catalytically active high dispersed metal.[10,11] It is known that obtain optimal
42 catalytic FT performance both high surface area and a well-developed porosity are very important for
43 achieving a high dispersion of the active phase in the catalyst. Carbon materials, especially AC, has surface
44 areas significantly higher than another conventional oxide catalyst supports increasing surface area and
45 porosity of the carbon facilitates the loading of metal [12]. As a chemically inert material, carbon support can
46 reduce the interaction with the cobalt species and increase the cobalt reducibility [13]. Advantageously
47 carbon materials can be prepared from residual biomass and waste materials which is an attractive property
48 for decreasing the so-called "carbon footprint" of a biomass transformation process [2]. Beside the high
49 surface area carbon support also has many other advantages in the catalytic applications like tailored pore
50 size distribution that can be modified for specific reactions, resistance to acidic or basic media, amphoteric
51 character due to the presence of various oxygenated functional groups which enhances metal adsorption
52 and catalyst dispersion, the structure that is stable at high temperatures, even above 700 °C (except in the

53 presence of oxygen >200 °C and for hydrogenation reactions >400 °C), less expensive compared to alumina
54 and silica supports; porous carbons can be prepared in different physical forms (granules, extrudates, pellets,
55 fibers, cloths, etc.), hydrophobic carbon can be modified to increase the hydrophilicity and active phase can
56 be recovered by eliminating the support through burning away the carbon. [2]

57 By modifying the carbon support, surface pore structure and functional groups (O, N, H) supported Co-
58 catalysts with a high degree of reduction and high Co dispersion can be obtained. These functional groups
59 are considered anchoring sites for cobalt particles on the surface of AC, which can increase the cobalt metal-
60 loading, dispersion, and stability.[13] It has been observed that the more acidic the groups are, the less
61 hydrophobic is the carbon surface, making the surface more accessible to the aqueous solution of the metal
62 precursor upon impregnation. The metallic dispersion is said to increase with the increased amount of oxygen
63 on the surface. Oxygen groups on the surface have been most studied since they are formed spontaneously
64 by exposure of the material to the atmosphere during the activation process. The concentration of these
65 groups can be increased with different oxygenation treatments such as nitric acid disposal. Fixation of the
66 acidic groups on the surface of the AC makes the surface more hydrophilic, decreases its pH, and increases
67 the negative surface charge density. These treatments can also affect the surface area and pore texture of
68 the activated carbons. [12, 14, 15]

69 Mesopore volume and mean mesopore size have been reported to be important parameters to control metal
70 particle size and dispersion on carbon materials. A support with modified mesoporous and macroporous
71 structure can have excellent advantages in FT reaction because larger pores benefits rapid molecular
72 transportation and enhances the production for longer hydrocarbon chain distribution. The microporous
73 structure of activated carbon is claimed to result in high methane and light hydrocarbon selectivity. [13,16]

74 A number of studies have been shown that addition of noble metals has a strong impact on the activity and
75 selectivity on cobalt catalysts. The addition of noble metal promoters can shift the temperature needed to
76 reduce cobalt oxide to metallic cobalt to lower temperatures, but its effect on the degree of reduction has
77 been reported to be rather minor. Instead, the improved activity of noble metal promoted cobalt catalysts
78 has been mainly attributed to higher cobalt dispersions. [17-19]

79 Many activated carbons have reported having high ash content. Ash content has a relatively small, but
80 significant negative effect on the adsorption of the metal precursor. By selecting an appropriate precursor
81 and modifying the carbon with different treatments, it is possible to prepare porous carbons with very low
82 ash content. [2, 3]

83 Preparation of carbon supported metal catalyst can be done with impregnation methods, precipitation
84 methods or by ion-exchange method. With impregnation methods, incipient wetness method is performed
85 in which the metal precursor is dissolved in small amount of solvent just enough to fill the pores of the
86 support. Cobalt-based catalysts are relatively seldom prepared with precipitation methods but few papers
87 have been published. [20-24]

88 In this study, a series of unpromoted and promoted cobalt catalysts supported on AC used as such or modified
89 by different acid treatments have been prepared and characterized. Effect of acid pretreatments (HCl and
90 HNO₃) on AC and different preparation methods including impregnation methods and precipitation methods
91 have been studied. Also, the effect of promoting the cobalt catalysts with noble metals ruthenium and
92 rhenium have been tested in this study.

93

94 **2. Experimental**

95 ***2.1 Preparation of activated carbon***

96 The lignin was dried and sieved to obtain particles of 0.8-1.2 mm in diameter. The sieved lignin was
97 carbonized and steam activated in a one-step process in a rotating quartz reactor (Nabertherm GmbH RSRB
98 80). The thermal profile during the whole process was divided into two parts: the first carbonization step, in
99 which the temperature was raised to 800 °C with a ramp of 6.7 °C /min, procured the total carbonization of
100 the lignin followed by the activation step. During the activation temperature was kept at 800 °C for 120 min
101 with a stream of water steam (120 g/h at 140 °C), created the proper surface activation. During the whole
102 process, the reactor was flushed with an inert gas, in ramping step only N₂ (flow 200 ml/min) and in activation
103 step carrier gas (N₂ flow 200 ml/min) and steam (120 g/h at 140 °C). The resulting AC was characterized for
104 ash content, carbon content (TC), specific surface area, and pore size distribution.

105

106 **2.2 Preparation of catalysts**

107 The formed AC was crushed and fractioned by sieving into particle size 50-100 μm . Some of the carbon was
108 used as such, other parts either acid-treated with hydrochloric acid (HCl) in order to demineralize the sample
109 or oxidized with nitric acid (HNO_3) in order to introduce functional groups into the carbon. Acid treatments
110 were performed with 30 wt. % HCl or with 10 wt. % HNO_3 refluxed 3h and washed with distilled H_2O until pH
111 was neutral. Finally, the AC was dried overnight at 105 $^\circ\text{C}$. AC demineralized with HCl was used as a support
112 in the preparation of catalyst AC-HCl-Co-IW and AC oxidized with HNO_3 was used as a support in the
113 preparation of catalysts AC- HNO_3 -Co-IW. AC-Co-IW was prepared by incipient wetness impregnation of
114 cobalt as such without any pretreatment of AC. Cobalt catalysts containing 10 wt. % of Co were prepared by
115 incipient wetness impregnation of the ACs using $\text{Co}(\text{NO}_3)_3 \cdot 6 \text{H}_2\text{O}$ as a precursor. Promoter metals ruthenium
116 or rhenium were added in some catalysts using precursor metal salts $\text{Ru}(\text{NO})(\text{NO}_3)_3$ (AC-CoRu-IW) or ReO_4H
117 (AC-CoRe-IW) in order to get 0.2 wt. % promoter metal on the catalyst. Promoter metal was added to
118 precursor solution and performed one-step incipient wetness impregnation. After impregnation, the
119 catalysts were dried overnight at 105 $^\circ\text{C}$ and calcined at 320 $^\circ\text{C}$ for 16 hours. The calcination step was
120 performed in a quartz reactor placed into a tubular oven and flushed with nitrogen (240 ml/h/ g_{cat}) during the
121 whole process. Beside incipient wetness impregnation method, precipitation method was used in the
122 preparation of AC-Co-PR catalyst. The cobalt precursor $\text{Co}(\text{NO}_3)_3 \cdot 6 \text{H}_2\text{O}$ was dissolved in distilled H_2O together
123 with urea in a molar ratio of cobalt to urea of 1:2, and AC. The resulting solution was heated to 80 $^\circ\text{C}$ and
124 stirred overnight to precipitate the cobalt. Finally, the impregnated AC was dried overnight at 105 $^\circ\text{C}$ before
125 calcination. With catalyst AC-Co-US, ultrasonic assisted impregnation method was performed using an
126 ultrasonic bath (VWR USC 200 TH, 45 kHz) during the addition of precursor solution ($\text{Co}(\text{NO}_3)_3 \cdot 6 \text{H}_2\text{O}$ dissolved
127 in water) with a total US exposure time equal to 60 min at room temperature. After sonication, catalyst was
128 rotated overnight in a rotating mixer (Rotavapor) and then dried overnight at 105 $^\circ\text{C}$. The calcination step
129 was performed in the same way for all catalysts as described above. A summary of the catalysts prepared
130 and the preparation methods of Co/AC-catalysts are presented in Table 1 and Figure 1.

131

132 **2.3 Catalyst characterization**

133 The resulting catalysts (see Table 1) were characterized by a number of methods including elemental analysis,
134 nitrogen physisorption, ICP-OES, SEM, TEM, DRIFT, XPS, XRD, and TPR analysis.

135

136 **2.3.1 Total carbon and ash contents**

137 The percentage of total carbon present in prepared ACs was measured using Skalar Primacs MCS instrument.
138 Dried samples were weighted in quartz crucibles, combusted at 1100 °C in a pure oxygen atmosphere and
139 the formed CO₂ was analyzed by an IR analyzer. The total mass of carbon in each sample was calculated as a
140 percent of the mass initially weighted.

141 All samples were analyzed for ash content. A known amount of AC was transferred to tared crucibles and
142 combusted in a muffle furnace for two hours at 815 °C with an initial temperature ramp of 9 °C /min. The ash
143 contents were calculated as a percent of the initial dried biomass.

144

145 **2.3.2 Surface areas and pore distribution**

146 Specific surface areas and pore size distributions were calculated from adsorption isotherms of N₂ at
147 isothermal conditions in liquid nitrogen according to the BET (Brunauer–Emmett–Teller) theory. Pore
148 distribution was calculated from the adsorption isotherms using the BJH (Barrett–Joyner–Halenda) method.
149 Each sample (about 100mg) was weight in a quartz tube. Samples were evacuated and heated in order to
150 remove any adsorbed components and moisture. Evacuated samples were measured under isothermal
151 conditions by Micromeritics ASAP 2020.

152

153 **2.3.3 Metal content, dispersions and particle sizes**

154 Metal contents of samples were measured by inductively coupled optical emission spectrometry (ICP-OES)
155 using a Perkin Elmer Optima 5300 DV ICP–OES instrument. 0.10-0.12 g samples were added in 37 %

156 hydrochloric acid and 63 % nitric acid, then digesting in a microwave oven (MARS, CEM Corporation) at 200
157 °C for 10 min. After digestion, the solution was diluted to 50 ml and measured by ICP-OES.

158 Metal dispersions and particle sizes were measured from calcined samples by chemisorption of carbon
159 monoxide (CO) assuming that stoichiometric ratio of was 1:1 between the adsorbent and cobalt (CO: Co) [25-
160 26]. Each sample (about 500 mg) was weight in a U-shaped quartz tube and the sample was supported with
161 glass wool. Prior to measurements, the sample was evacuated followed by a reduction in a stream of
162 hydrogen (H₂) at 350 °C. Measurements were done using a Micromeritics ASAP 2020.

163

164 **2.3.4 Catalyst morphology**

165 A field emission scanning electron microscope (FESEM) Zeiss Ultra Plus equipped with and energy-dispersive
166 X-ray spectroscopy (EDS) analysis system at the Center of Microscopy and Nanotechnology, University of
167 Oulu was used to study the microstructure of the catalysts and for elemental analyses.

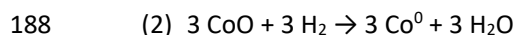
168 The morphology of the catalyst particles dispersed in the microemulsion was studied using an energy filtered
169 transmission electron microscope EFTEM (LEO 912 OMEGA EFTEM). The catalysts samples were dispersed in
170 acetone and pretreated in an ultrasonic bath for several minutes. A small drop of the microemulsion was
171 deposited on a copper grid pre-coated with carbon and then evaporated in air at room temperature. The
172 particle size of the samples was measured from TEM images of each sample and given in a reasonable range.
173 The accelerating voltage and emission current in the measurements were 120 kV and 8-15 µA, respectively,
174 while the resolution of the instrument was 0.37 nm.

175 X-ray diffraction (XRD) patterns were recorded by a PANalytical X'Pert Pro X-ray diffraction equipment using
176 monochromatic CuKα₁ radiation ($\lambda=1.5406 \text{ \AA}$) at 45 kV and 40 mA. Diffractograms were collected in the 2 θ
177 range 5-80° at 0.017° intervals and with scan step time of 110 s. The crystalline phases and structures were
178 analyzed by HighScore Plus.

179

180 **2.3.5 Temperature programmed reduction and oxidation**

181 The conventional temperature programmed reduction experiments (TPR) were performed using a
182 Thermoquest Mod. TPR/D/O 1100 (TCD detector) by feeding 30 ml/min of a 5.1% v/v H₂ in Ar gas mixture
183 while heating by 8 °C/min from 50 °C up to 900 °C. The samples have been initially pre-treated in a flow of
184 argon at T= 200 °C for 0.5 h. The TPR profiles of the catalysts exhibit hydrogen consumption peaks attributed
185 to two-step reduction of Co₃O₄ to metallic cobalt with intermediate phase consisting mainly of CoO but most
186 likely other hard-reduced cobalt oxides are present in the second peak.



189 The degree of reduction for the catalysts was measured on a Micromeritics Autochem by reoxidation of
190 reduced catalysts. Small portions, about 25 mg, of each catalyst were weighed into a quartz tube. Prior to
191 analysis, the samples were dried at 100 °C for 1 hour and then reduced for 1 hour at 350 °C in a flow of 10 %
192 H₂ in Ar according to reactions (1) and (2). Co surface was rinsed with He flow until the signal from the TCD
193 detector returned to the baseline. Small pulses of oxygen (5 % in He) were added using a calibrated loop until
194 signals with a constant area were obtained. Between the pulses, the signal was allowed to return to baseline
195 before applying next pulse. The degree of reduction was calculated from the moles of oxygen consumed
196 assuming that all Co⁰ was oxidized to Co₃O₄ according to reaction (3) compared to the amount of oxygen
197 theoretically needed for a complete re-oxidation of Co⁰. Any oxidation of the promoter metals or other
198 reductions/ oxidations of other Co-species were not considered in the calculations.



200

201 **2.3.6 X-ray photoelectron spectroscopy**

202 X-ray photoelectron spectroscopy (XPS) analysis was performed using a Thermo Fisher Scientific ESCALAB
203 250Xi XPS System at the Center of Microscopy and Nanotechnology, University of Oulu (Finland). The catalyst
204 samples were placed on an Indium film. With pass energy of 20 eV, the spot size of 900 μm, the accuracy of
205 the reported binding energy was ±0.2 eV. The Al, O, Co, Re or Ru, C, In and N were measured for all samples.

206 The measurement data were analyzed by Avantage V5. The monochromatic AlK α radiation (1486.7 eV)
207 operated at 20 mA and 15 kV. Charge compensation was used to determine the presented spectra and the
208 calibration of the binding energies (BE) were performed by applying the C1s line at 284.8 eV as a reference.

209

210 ***2.3.7 The Diffuse Reflectance Infrared Fourier Transform***

211 The Diffuse Reflectance Infrared Fourier Transform (DRIFT) analyses were performed by Brüker PMA 50
212 Vertex 80v equipment. In the DRIFT measurements the sample was maintained in a nitrogen flow at 105 °C
213 for 60 min for the removal of water, then the chamber was cooled down to 25 °C in a nitrogen atmosphere,
214 Analyses resolution was 4 cm⁻¹ and 100 scans/min. Activated carbon samples were mixed with KBr (1:300) in
215 a mortar to obtain a homogenous powder.

216

217 **3. Results and discussion**

218 ***3.1 Characterization results***

219 Characterization results of untreated and treated samples are presented in Table 2. The table presents
220 surface areas, pore sizes, pore volumes, and distributions. Also, total carbon content and ash contents are
221 presented in Table 2. According to these analyses, carbonization and steam activation increased the carbon
222 content of the Kraft lignin remarkable. Surface area (see Table 2) increased from 4.6 to 810 m²/g and carbon
223 content from 65 to 96 %. According to ash content, treatment with acid removed ash/minerals from the AC.
224 Treatment with HCl seemed to remove some ash (from 6.1 to 4.8 %) and treatment with HNO₃ removed all
225 remaining (from 6.1 to 0.0 %) ash from the AC. HNO₃ treatment seemed to collapse some of the carbon
226 structure observed from decreasing surface area, pore volume, and total carbon content. Instead, HCl
227 treatment seemed to open some of the carbon pore structure that could be seen from the slight increase in
228 BET surface area.

229 The surface area of AC produced from Kraft lignin was rather high, 810 m²/g, (see Table 2) compared to
230 conventionally used supports which surface area is approximately 200 m²/g or less [27-29]. Pore distribution

231 according to BJH model of AC (see Table 2) was 32 % of micropores (diameter smaller than 2 nm), 62 % of
232 mesopores (diameter from 2 nm to 50 nm) and 6 % of macropores (diameter larger than 50 nm).

233 Elemental analysis (C, H, O, N) was performed for activated carbon samples before Co addition and a
234 summary of these results is presented in Table 3. Results from the elemental analysis showed that treatments
235 with acid HNO₃ and HCl increased the amount of hydrogen in the carbon support. Treatment with HNO₃
236 increased nitrogen content in the AC support but the amount of oxygen decreased to zero. According to the
237 literature, treatment with HNO₃ will increase oxygen at the carbon surface. In the results obtained from the
238 elementary analyses, no such increase could be measured.

239 Surface area, pore volume, pore size, cobalt metal dispersion, metal particle size and metal surface area of
240 prepared and calcined Co/AC-catalysts are presented in Table 4. Impregnation with metal precursor
241 decreased the BET surface area about 10-26 % within range AC-HNO₃-Co-IW< AC-Co-IW< AC-Co-PR< AC-
242 CoRe-IW< AC-CoRu-IW< AC-HCl-Co-IW< AC-Co-US. Pore volumes decreased about 10-32 % within range AC-
243 HNO₃-Co-IW< AC-Co-IW< AC-Co-PR< AC-CoRu-IW <AC-CoRe-IW< AC-HCl-Co-IW< AC-Co-US. With catalyst AC-
244 Co-US and AC-HCl-Co-IW, the BET surface areas and pore volumes decreased most (BET surface areas 26 %
245 and pore volumes 32-27 %). Since the decrease of the surface areas and pore volumes were in some cases
246 quite high it seems an indication to that there might be some other compounds involved for example nitrates
247 from the precursor. Also, there is a possibility that some treatments e.g. US might collapse some of the AC
248 surface structure.

249 According to CO-chemisorption results dispersion of cobalt ranged from 0.7-10.1 % (see Table 4) within range
250 AC-HCl-Co-IW< AC-CoRu-IW< AC-HNO₃-Co-IW< AC-CoRe-IW< AC-Co-IW< AC-Co-US. Compared to previous
251 studies [29] with conventional supported (Al₂O₃, SiC, TiO₂) cobalt dispersion in Co/AC-catalysts was quite
252 competitive and in some cases rather high, especially with catalyst AC-Co-US dispersion of Co was even high
253 as 10.1 %. Also, catalyst AC-Co-IW gave quite high values for the dispersion of cobalt metal, 8.6 %. Otherwise,
254 it was expected, and as it was discussed in introduction part that oxidation treatment leads to a higher
255 dispersion; treatment with HNO₃ did not lead any particularly high cobalt dispersion on the surface and the

256 metal dispersion of catalyst AC-HNO₃-Co-IW was 3.4 %. The reason for this might be that treatment with
257 HNO₃ did not increase the oxygen content of the AC. Instead, treatment with HCl increased oxygen content
258 in the AC (see Table 3) but also in this case no higher metal dispersion was observed, in fact, HCl treated AC
259 proved to have the lowest dispersion from prepared Co/AC-catalysts. According to CO-chemisorption results
260 addition of promoter metals did not give any particularly high metal dispersion and Ru- and Re-promoted
261 catalysts were measured to have a metal dispersions of 3.2 % (AC-CoRu-IW) and 5.8 % (AC-CoRe-IW)
262 respectively.

263 Metal contents of the catalysts were measured by ICP analysis. The expected concentration of cobalt added
264 was 10 wt. % and concentration of ruthenium and rhenium were 0.2 wt. %. The measured concentrations of
265 metals are presented in Table 5. Cobalt concentrations in catalysts were at the expected level around 10 wt.
266 % except in catalyst AC-Co-IW which contained only 5.9 wt. % of cobalt. The reason for this might be the
267 preparation step and miscalculation the amount of cobalt. The concentration of promoter metals was
268 expected to be 0.2 wt. %. The concentration of promoter Ru was in desired concentration, 0.24 wt. %.
269 Measured value of Re was 0.39 wt. %. This double sized value must have caused the preparation step in
270 which the addition of a very small amount of liquid promoter was difficult. Other metals including calcium,
271 iron, potassium, sodium and magnesium were also measured to verify if some traces of metal were left from
272 the preparation process of AC. Acid treated catalysts AC-HCl-Co-IW and AC-HNO₃-Co-IW contained these
273 metals less than 0.02%. The concentration of metal Ca was 0.02 wt. % and concentration of metals Fe, Na, K
274 and Mg were 0.01 wt. % or less and could be expected that no interference from these metals should be
275 present in catalytic use. Other catalysts (AC-Co-IW, AC-CoRu-IW, AC-CoRe-IW, and AC-Co-US) contained Ca
276 <0.04 wt. %, Fe <0.06 wt. % and Mg <0.03 wt. % and these values were quite low. Instead, concentrations of
277 Na and K were higher; Na <0.35 wt. % and K <0.11 wt. %. These metals might be traces from pulping process
278 and might interfere the catalytic activity in a negative way. [30, 31]

279 SEM and TEM analyses were used to verify catalyst morphology. From FESEM and TEM images (Figure 2)
280 taken from the catalyst AC-Co-IW can be observed that Co-particles size were around 10-20 nm which was

281 quite close to results from CO-chemisorption in which average Co particle size was determined to be 11.6
282 nm (Table 4). TEM images of AC-Co-IW also highlighted that the active metal was present in the form of
283 spherical particles with dimensions of about 10-20 nm quite well distributed on the support surface.

284 SEM-EDS analyses were performed for calcined Co/AC-catalysts. The point analyze were performed at
285 different locations and marked in the SEM images. All elements were auto-detected using Oxford
286 Instruments INCA software. Figure 3 showed the SEM-EDS analyze sites for catalyst AC-HNO₃-Co-IW. From
287 SEM-EDS analyses, only major components (C, O and Co) are shown in Table 6. The SEM-EDS analyses also
288 indicated the addition of Co on the catalyst surface.

289 XRD measurements were performed for calcined but not reduced Co/AC-catalysts. XRD was used to confirm
290 the presence of cobalt in the catalysts and also to verify metal particle size. From XRD diffraction patterns, it
291 was observed that catalysts showed very broad peaks for Co oxides, indicating a high cobalt metal dispersion
292 and/or amorphous phase of support [32,33]. Since the broad peaks detected from XRD patterns calculation
293 of cobalt metal particle size, based on Scherrer equation was not reliable. However from the XRD diffraction
294 pattern (Figure 4) broad peaks indicated to CoO (111) at 2theta=36.7° and CoO (200) at 2theta=42.6°,
295 according to standard JCPDS file number (CoO 04-005-4912) which proved the presence of cobalt in catalysts.

296

297 **3.2 Reducibility of catalysts**

298 **3.2.1 Temperature programmed reduction (TPR)**

299 According to the literature [34] from the H₂-TRP profile of Co/AC-catalysts three major peaks could be found;
300 the first peak at around 320 °C corresponding the reduction of Co₃O₄ to CoO and second high-temperature
301 peak at 450 °C related to the reduction of CoO to metallic cobalt, the third broad peak maximum around 600
302 °C is attributed to methane formation which is originated from the reduction of surface functional groups on
303 the AC surface by H₂. From the H₂-TRP profile (Figure 5) in some cases, a small peak at 100 °C was detected
304 which is due to desorption of residue moisture adsorbed on the catalysts surface. Also, the weak reduction

305 peak at around 220 °C could be found and is due to decomposition of residual cobalt nitrate. The first
306 reduction peak for all catalysts is found at temperature 320-380 °C and the intensity is about the same for
307 all. With second peak reduction step corresponding to the reduction of CoO and cobalt oxides to Co⁰ there is
308 more variety with reduction temperatures from 370 to 490 °C. A summary of H₂-TPR reduction temperature
309 shifts is presented in Table 7. The treatment with HNO₃ (AC-HNO₃-Co-IW) seemed to shift the second
310 reduction step to a lower temperature at 370 °C

311 The influence of support material and interaction between support and metal oxide can be observed when
312 AC supported catalysts was compared to the conventional SiO₂ supported catalyst synthesized and
313 characterized in a previous work [35]. Carbon supported catalysts presented little higher reduction
314 temperatures referred to the first reduction step with respect with traditional FT catalysts [36, 37]. The first
315 peak of reduction Co₃O₄ to CoO was around 260 °C for silica supported (SiO₂-Co) and 320-380 °C for AC
316 supported Co-catalysts while second peak related to the reduction of CoO to metallic cobalt showed
317 remarkable lower temperature for AC supported catalysts compared to silica supported catalyst (SiO₂-Co), in
318 fact, the average temperature of carbon supported catalyst is around T= 420 °C, while the reduction
319 temperature for the transition from CoO to Co presented by the SiO₂ supported catalysts is equal to T= 780
320 °C due to the presence of Co-silicates species, which are hard reducible species [38].

321

322 **3.2.2 Temperature programmed oxidation (TPO)**

323 The degree of reduction (Table 8) was calculated from the theoretical value of moles of oxygen per consumed
324 moles of oxygen using the measured Co metal content value from the ICP analysis (see Table 5). The addition
325 of Re seemed to affect the reduction degree of the catalyst AC-CoRe-IW with the highest degree of reduction
326 72 %. Catalyst AC-HNO₃-Co-IW oxidized with HNO₃ had a degree of reduction 66 %. With catalyst AC-CoRe-
327 IW, the degree of reduction was higher when compared to conventional CoRe-catalyst supported on Al₂O₃
328 from literature [39]. The lowest degree of reduction was calculated on catalysts AC-Co-US and it was equal
329 to 25 %. Low values of reduction were measured also with catalysts AC-CoRu-IW (38 %) and AC-Co-IW (39

330 %). One of the reasons for the low degree of reduction might be explained due to rather small cobalt particle
331 sizes, which are harder to reduce. Overall, these values were well comparable with other tested Co/AC-
332 catalysts from the literature [40].

333

334 **3.3 Surface functional groups**

335 Functional groups of activated carbon surface were determined by diffuse reflectance Fourier transformed
336 IR (DRIFT) analysis and it was possible to identify some of the oxygen-containing functionality. One of the
337 problems using infrared spectroscopy (FTIR) of carbonaceous materials is that they are effective black body
338 absorbers and are too opaque for direct transmission analysis on the mid-infrared spectral region. The
339 addition of KBr intensifies the signal but the signal is still too weak to obtain. An alternative technique is to
340 use (DRIFT) [41, 42]. Although IR spectroscopy does not provide quantitative information about carbon
341 surface chemistry, it can identify groups created or destroyed. Produced AC's were compared with
342 commercial AC. Main peaks at area 3400 cm^{-1} , 1620 cm^{-1} and 1620 cm^{-1} can be found from all AC's. From the
343 spectrum (Figure 6), few changes with different AC's peaks can be detected at the area $1000\text{-}2000\text{ cm}^{-1}$.
344 Notable changes with peaks from AC treated with HNO_3 were at area 1760 cm^{-1} (carbonyl stretching of
345 quinones and carboxylic acids), 1590 cm^{-1} (C=C stretching in the form of aromatic rings) and 1240 cm^{-1} (C-O
346 stretches presumably from both carboxylic acid groups and phenolic hydroxyls) [43, 44]. Peaks at 1570 cm^{-1} ,
347 1380 cm^{-1} and 1240 cm^{-1} might also indicate to C=N structure[23].

348 XPS measurements were performed for calcined but not reduced Co/AC-catalysts to get more specific
349 information from functional groups on activated carbon, especially carbon-oxygen, and cobalt complexes.

350 Figure 7a shows the high resolution C1s-spectra and reveals components corresponding carbidic carbon ($BE=$
351 $282.6\text{-}282.9\text{ eV}$); graphitic or aliphatic carbon ($BE= 284.6\text{-}285.1\text{ eV}$); carbon species in alcohol or ether groups
352 ($BE= 286.3\text{-}287.0\text{ eV}$); carbon in carbonyl groups ($BE= 287.5\text{-}288.1\text{ eV}$); carbon in carboxyl or ester groups
353 ($BE= 289.3\text{-}290.0\text{ eV}$); and shake-up satellite due $\pi\text{-}\pi^*$ transition in aromatic rings ($BE= 291.2\text{-}292.1\text{ eV}$). Peaks

354 in the region 286.3-287.5 eV may also present of structures C-N [45, 46]. From Table 9 can be seen that most
355 of the carbon atoms present in the catalyst are graphitic/aliphatic and about 15-20 % is in carbon-oxygen (or
356 C-N) compounds.

357 XPS spectrum of O1s-scans is presented in Figure 7b. and represents the oxygen groups on the surface of the
358 catalyst. In the O1s-spectra functional oxygen groups are divided in three different peaks representing double
359 bonded oxygen (C=O) to carbon in carbonyl, carboxyl, oxygen of quinone groups ($BE= 530.4-530.8$ eV); single
360 bonded oxygen (C-O) in alcohol or ester groups ($BE= 532.4-533.1$ eV) and chemisorbed oxygen or water ($BE=$
361 $534.8-535.6$ eV). Results showed that oxygen is in the form of double bonded oxygen and single bonded
362 oxygen quite evenly (Table 9). Moreover, catalyst AC-Co-US contained more of double bonded oxygen
363 (carbonyl/carboxyl) compounds than other catalysts while catalyst AC-HNO₃-Co-IW contained the least
364 oxygen-containing groups from the catalysts.

365 XPS results of N1s-scans are presented in Table 9. The intensities of peaks from N1s spectrum was low but
366 showed that catalysts AC-Co-PR and AC-HNO₃-Co-IW contained more nitrogen than other catalysts.

367 The Co2p-scan XPS results of the catalysts (Figure 7c) highlighted that, as already confirmed by the TPR, Co
368 is present in its oxidized forms Co₃O₄, Co₂O₃ and CoO ($BE= 779-782$ eV) and no Co⁰ ($BE= 778$ eV) has been
369 found in any of the catalysts [47]. The lack of metallic Co is attributable to the fact that the Co-precursor used
370 has an oxidation state equal to +3 and no further reduction treatments have been applied before XPS
371 analysis.

372 Figure 8 highlights that the treatment with ultrasound causes a huge decrease in the content of graphitic or
373 aliphatic carbon in AC-Co-US catalyst. It is wide discussed that ultrasounds are capable of degrading carbonyls
374 and moreover a suitable technique to degrade graphite into other compounds [48, 49].

375 **4. Conclusions**

376 A series of Co-based catalysts supported on activated carbon and eventually promoted with Ru or Re have
377 been synthesized and characterized. Different pretreatments and metal addition procedures seemed to have
378 a high impact to the prepared Co-catalyst.

379 Prepared carbon support seemed to have many attractive properties including high specific surface area,
380 proper pore distribution and high volume of mesopores and rather low ash value, which could be decreased
381 even to zero by acid treatment. Acid treatment seemed to be important for removing inorganic compounds
382 e.g. metals from the carbon support, which might affect to catalytic activity. Analyses including ICP-OES, SEM,
383 TEM and XRD indicated that cobalt was successfully added onto carbon support in all catalyst preparation
384 cases.

385 Some of the prepared Co-catalysts seemed to have good qualities (for FT-catalyst). Rather high dispersion
386 (10.1 %) of the active metal (cobalt) was measured with Co-catalyst prepared by ultrasonic assisted
387 impregnation method. Otherwise, there was an indication that a small metal particle size was difficult to
388 reduce (TPO). TPR results highlighted that carbon supported cobalt catalysts proved to have lower reduction
389 temperatures referred to the second reduction step of cobalt oxide to metallic cobalt if compared with SiO₂
390 supported FT catalyst. Moreover, pretreatment with HNO₃ seemed to have a positive effect on reduction
391 temperatures and to a degree of reduction compared to other prepared Co/AC-catalysts. Also, the addition
392 of the promoter Re did seem to improve the reduction degree of cobalt as measured in the TPO
393 measurements. According to XPS analyses, different preparation techniques seemed to have an impact on
394 the catalyst surface structure. Further, these prepared cobalt catalysts needs a thorough testing in the pilot
395 scale FT plant.

396

397 **5. Acknowledgements**

398 The authors acknowledge the EU/European Regional Development Fund, Leverage from the EU program
399 (within project nr. A71029) for financial support.

400

401 **6. References**

- 402 [1] Demirbaş A, Arslan G, Pehlivan E (2006) Energy Sources, Part A: Recovery, Utilization, and
403 Environmental Effects 28:627-638
- 404 [2] Lam E, Luong JHT (2014) ACS Catalysis 4:3393-3410
- 405 [3] Rodríguez-Reinoso F (1998) Carbon 36:159-175.
- 406 [4] Bezemer GL, Radstake PB, Falke U, Oosterbeek H, Kuipers HPCE, van Dillen AJ, et al. (2006) Journal of
407 Catalysis 237:152-161.
- 408 [5] Khodakov AY (2009) Catalysis Today 144:251-257
- 409 [6] Jean-Marie A, Griboval-Constant A, Khodakov AY, Diehl F (2009) Comptes Rendus Chimie 12:660-667
- 410 [7] Tsakoumis NE, Rønning M, Borg Ø, Rytter E, Holmen A (2010) Catalysis Today 154:162-182
- 411 [8] Iglesia E (1997) Applied Catalysis A: General 161:59-78
- 412 [9] Gnanamani MK, Jacobs G, Shafer WD, Davis BH (2013) Catalysis Today 215:13-17
- 413 [10] van Steen E, Prinsloo FF (2002) Catalysis Today 71:327-334
- 414 [11] Zaman M, Khodadi A, Mortazavi Y (2009) Fuel Processing Technology 90:1214-1219
- 415 [12] Serp P, Machado B (2015) Carbon (Nano) Materials for Catalysis, Nanostructured Carbon Materials for
416 Catalysis, the Royal Society of Chemistry, pp. 1-45
- 417 [13] Fu T, Li Z (2015) Chemical Engineering Science 135:3-20
- 418 [14] Bitter JH, de Jong KP (2008) Preparation of Carbon-Supported Metal Catalysts, In: Serp P, Figueiredo JL
419 (Eds) Carbon Materials for Catalysis. John Wiley & Sons, Inc., pp. 157-176
- 420 [15] Moreno-Castilla C, Ferro-Garcia MA, Joly J P, Bautista-Toledo I, Carrasco-Marin F, Rivera-Utrilla J (1995)
421 Langmuir 11:4386-4392
- 422 [16] Kang J, Zhang S, Zhang Q, Wang Y (2009) TOC 121:2603-2606
- 423 [17] Kogelbauer A, Goodwin JG, Oukaci R (1996) Journal of Catalysis 160:125-133
- 424 [18] Eschemann TO, Oenema J, de Jong KP (2016) Catalysis Today 261:60-66
- 425 [19] Jacobs G, Das TK, Zhang Y, Li J, Racoillet G, Davis BH (2002) Applied Catalysis A: General 233:263-281
- 426 [20] Shu S, Guo J, Liu X, Wang X, Yin H, Luo D (2016) Applied Surface Science, Part B 360:684-692
- 427 [21] Zabihi M, Khorasheh F, Shayegan J (2015) Reaction Kinetics, Mechanisms and Catalysis 114:611-628
- 428 [22] Munnik P, de Jongh PE, de Jong KP (2015) Chemical Reviews 115:6687-6718
- 429 [23] Serp P, Joseph JL (2009) Carbon Materials for Catalysis, Wiley, Canada

- 430 [24] Khodakov AY, Chu W, Fongarland P (2007) *Chemical Reviews* 107:1692-1744
- 431 [25] Zowtiak JM, Bartholomew CH (1983) *Journal of Catalysis* 83:107-120
- 432 [26] Reuel RC, Bartholomew CH (1984) *Journal of Catalysis* 85:63-77
- 433 [27] Kababji AH, Joseph B, Wolan JT (2009) *Catalysis Letters* 130:72-78
- 434 [28] Maitlis MP, de Klerk A (2013) *Greener Fischer-Tropsch Processes for Fuels and Feedstocks*, Wiley-VCH
- 435 [29] Romar H, Lillebo AH, Tynjala P, Hu T, Holmen A, Blekkan EA, Lassi U (2016) *Journal of Materials Science*
436 *Research* 5:39-49
- 437 [30] Tsakoumis NE, Rønning M, Borg Ø, Rytter E, Holmen (2010) *A Catalysis Today* 154:162–182
- 438 [31] Lillebø AH, Patanou E, Yang J, Blekkan EA, Holmen A (2013) *Catalysis Today* 215:60–66
- 439 [32] Song X, et al. (2013) *Applied Catalysis A: General Volume* 452:155–162
- 440 [33] Beswick O, et al. (2017) *Catalysis Today* 279, Part 1:29–35
- 441 [34] Wang T, Dinga Y, Xionga J, Yana L, Zhua H, Lua Y (2006) *Catalysis Letters* 107:47-52
- 442 [35] Comazzi A, Pirola C, Di Michele A, Compagnoni M, Galli F, Rossetti I, et al. (2016) *Applied Catalysis A:*
443 *General* 520:92-98
- 444 [36] Lin H, Chen Y (2004) *Materials Chemistry and Physics* 85:171-175
- 445 [37] Olusola OJ, Sudip M (2016) *Journal of Petroleum Technology and Alternative Fuels* 7:1-12
- 446 [38] Ming H, Baker BG (1995) *Applied Catalysis A: General* 123:23-36
- 447 [39] Borg Ø, et al. (2007) *Journal of Catalysis* 248:89-100
- 448 [40] Zhang, Y, et al. (2007) *Fischer-Tropsch synthesis, Catalysts and Catalysis*, Edit, Davis BH and Occelli ML,
449 p.87-99
- 450 [41] Jagiello J (1994) *Langmuir* 10:2778-2785
- 451 [42] Moreno-Castilla C, López-Ramón MV, Carrasco-Marín F (2000) *Carbon* 38:1995-2001
- 452 [43] Dandekar A, Baker R, Vannice M (1998) *Carbon* 36:1821-1831
- 453 [44] Mangun CL, Benak KR, Daley MA, Economy J (1999) *Chemistry of Materials* 11: 3476-3483
- 454 [45] Biniak S, Szymański G, Siedlewski J, Świątkowski A (1997) *Carbon* 35:1799-1810
- 455 [46] Nahil MA, Williams PT (2012) *Waste Biomass Valor* 3:117-130
- 456 [47] Biesinger MC, et.al (2011) *Applied Surface Science* 257:2717-2730

457 [48] Suslick KS, Hyeon T, Fang M, Cichowlas AA (1995) Materials Science and Engineering: A 204:186-192

458 [49] Guittoneau F, Abdelouas A, Grambow B, Huclier S (2010) Ultrasonics Sonochemistry 17:391-398

459

460

461

462

463

464

465

466

467

468

469

470

471

472

473

474

475

476

477 **Lahti et al. Table captions**

478

479 Table 1. A summary of catalyst denotation: precursor salts, impregnation methods and calcination.

480

481

482

483

484

485

486

487

488

489

490

491

492

493

494

495

496

497

498

499

500

501

502 Lahti et al. Tab 1.

503

Catalyst	Metal content	Metal salts used	Impregnation method used	Calcination
AC-Co-IW	10 wt. % Co	Co(NO ₃) ₂ ·6H ₂ O	incipient wetness	320°C, 16h, N ₂ -flow
AC-HCl-Co-IW*	10 wt. % Co	Co(NO ₃) ₂ ·6H ₂ O	incipient wetness	320°C, 16h, N ₂ -flow
AC-HNO ₃ -Co-IW**	10 wt. % Co	Co(NO ₃) ₂ ·6H ₂ O	incipient wetness	320°C, 16h, N ₂ -flow
AC-CoRu-IW	10 wt. % Co 0.2 wt. % Ru	Co(NO ₃) ₂ ·6H ₂ O Ru(NO)(NO ₃) ₃	one-step incipient wetness	320°C, 16h, N ₂ -flow
AC-CoRe-IW	10wt. % Co 0.2 wt. % Re	Co(NO ₃) ₂ ·6H ₂ O ReO ₄ H	one-step incipient wetness	320°C, 16h, N ₂ -flow
AC-Co-PR	10 wt. % Co	Co(NO ₃) ₂ ·6H ₂ O	precipitation with urea	320°C, 16h, N ₂ -flow
AC-Co-US	10 wt. % Co	Co(NO ₃) ₂ ·6H ₂ O	ultrasonic assisted incipient wetness	320°C, 16h, N ₂ -flow

504 *) AC demineralized with HCl and **) AC oxidized with HNO₃ before impregnation.

505

506

507

508

509

510

511

512

513

514

515

516

517

518 **Lahti *et al.* Table captions**

519 Table 2. Surface area, pore volume, pore size, pore distribution, total carbon content and ash content of
520 the raw lignin, activated carbon and acid treated activated carbons.

521

522

523

524

525

526

527

528

529

530

531

532

533

534

535

536

537

538

539 Lahti et al. Tab 2.

540

Sample	BET		Pore size (nm)	BJH pore distribution			Carbon content (%)	Ash (%)
	Surface area (m ² /g)	Pore volume (cm ³ /g)		Micro-pores (%)	Meso-pores (%)	Macro-pores (%)		
Lignin, untreated	4.6	0.02	18	n.d.	n.d.	n.d.	65	n.d.
AC	810	0.41	2	32	62	6	96	6.1
AC, treated with HCl	822	0.41	2	34	60	6	95	4.8
AC, treated with HNO ₃	714	0.35	2	33	61	6	85	0.0

541 n.d. = not determined

542

543

544

545

546

547

548

549

550

551

552

553

554 **Lahti et al. Table captions**

555

556 Table 3. Elemental analysis (C, H, O, N) for activated carbon supports.

557

558

559

560

561

562

563

564

565

566

567

568

569

570

571

572

573

574 Lahti et al. Tab 3.

575

Sample	Treatment	C (%)	H (%)	O (%)	N (%)
AC	Untreated	86.4	0.7	2.2	0.6
AC	30% HNO ₃ , reflux 3h	59.6	1.9	0	1.4
AC	30% HCl, reflux 3h	79.8	1.2	4.3	0.5

576

577

578

579

580

581

582

583

584

585

586

587

588

589

590 **Lahti *et al.* Table captions**

591

592 Table 4. Surface area, pore volume, pore size, cobalt metal dispersion, metal particle size and metal surface
593 area of Co/AC-catalysts.

594

595

596

597

598

599

600

601

602

603

604

605

606

607

608

609

610

611 Lahti et al. Tab 4.

612

613

Catalyst*	BET Surface area (m ² /g)	Pore volume (cm ³ /g)	Average pore size (nm)	Co metal dispersion (%)	Co metal particle size (nm)	Co metal surface area (m ² /g sample)	Co metal surface area (m ² /g of metal)
AC-Co-IW	710	0.35	2	8.6	11.6	5.8	58.1
AC- HCl-Co-IW	610	0.30	2	0.7	138.5	0.5	4.9
AC-HNO ₃ -Co-IW	640	0.32	2	3.4	29.8	2.3	22.7
AC-CoRu-IW	640	0.29	2	3.2	31.0	2.2	21.8
AC-CoRe-IW	630	0.31	2	5.8	17.2	3.9	39.2
AC-Co-PR	680	0.34	2	n.d.	n.d.	n.d.	n.d.
AC-Co-US	600	0.28	2	10.1	9.8	6.9	68.6

614 *) Preparation methods presented in Table 1.

615 n.d. = not determined

616

617

618

619

620

621

622

623

624

625

626

627 **Lahti *et al.* Table captions**

628

629 Table 5. Metal content in catalysts from ICP analysis.

630

631

632

633

634

635

636

637

638

639

640

641

642

643

644

645

646

647

648

649

650

651

652

653

654
655 Lahti et al. Table 5.

656
657

Catalyst	Co wt.%	Ru wt.%	Re wt.%	Ca wt.%	Fe wt.%	Na wt.%	K wt.%	Mg wt.%
AC-Co-IW	5.9			0.02	0.02	0.30	0.11	<0.01
AC-HCl-Co-IW	11.1			0.02	0.01	0.01	<0.01	<0.01
AC-HNO ₃ -Co-IW	8.3			0.02	0.01	0.01	<0.01	<0.01
AC-CoRe-IW	9.1		0.39	0.03	0.03	0.35	0.10	0.02
AC-CoRu-IW	9.3	0.24		0.04	0.06	0.13	0.07	0.03
AC-Co-PR	9.2			0.01	0.02	0.25	0.09	<0.01
AC-Co-US	9.8			0.04	0.06	0.21	0.07	0.03

658

659

660

661

662

663

664

665

666

667

668

669

670

671

672 **Lahti et al. Table captions**

673

674 Table 6. SEM-EDS spectrum labels from catalyst AC-HNO₃-Co-IW.

675

676

677

678

679

680

681

682

683

684

685

686

687

688

689

690

691

692 Lahti et al. Tab 6.

693

Spectrum Label	S147	S148	S149	S150	S151	S152	S153	S154	S155	S156
C	26.22	20.98	35.43	20.39	27.05	63.41	22.03	24.76	35.54	22.52
O	1.06	20.11	2.40	0.71	1.40	8.44	0.85	0.99	15.91	0.84
Co	71.82	58.53	60.49	75.82	70.36	27.39	76.10	72.67	48.19	75.32

694

695

696

697

698

699

700

701

702

703

704

705

706

707

708

709 **Lahti et al. Table captions**

710

711 Table 7. Temperatures (°C) for reduction steps and total H₂-consumption.

712

713

714

715

716

717

718

719

720

721

722

723

724

725

726

727

728

729 Lahti et al. Tab 7.

730

Catalyst	Phase transformation T (°C)		Total H ₂ -consumption (mmol/g _{cat})
	Co ₃ O ₄ →CoO	CoO→Co ⁰	
AC-Co-IW	330	480	4.0
AC-HCl-Co-IW	350	410	3.3
AC-HNO ₃ -Co-IW	320	370	6.3
AC-CoRu-IW	330	420	7.0
AC-CoRe-IW	380	480	5.2
AC-Co-PR	340	470	5.0
AC-Co-US	340	490	5.7
Co-SiO ₂	260	780	n.d.

731

732

733

734

735

736

737

738

739

740

741

742 **Lahti et al. Table captions**

743

744 Table 8. The degree of reduction at 350°C and volume of O₂ adsorbed on the catalyst surface.

745

746

747

748

749

750

751

752

753

754

755

756

757

758

759

760

761

762 Lahti et al. Tab 8.

763

Catalyst	O ₂ -consumption (ml/g _{cat})	Degree of reduction (%)
AC-Co-IW	1.2	39
AC-HCl-Co-IW	2.2	37
AC-HNO ₃ -Co-IW	1.9	66
AC-CoRu-IW	1.9	38
AC-CoRe-IW	2.2	72
AC-Co-PR	1.8	45
AC-Co-US	1.3	25

764

765

766

767

768

769

770

771

772

773

774

775

776

777 **Lahti et al. Table captions**

778

779 Table 9. Spectral parameters of C1s-, O1s-, Co2p- and N1s-scans of catalysts.

780

781

782

783

784

785

786

787

788

789

790

791

792

793

794

795

796

797

798

799

800

801 Lahti et al. Tab 9.

802

Scan	Binding Energy (eV)	AC-Co-IW (A%)	AC-HCl-Co-IW (A%)	AC-HNO ₃ -Co-IW (A%)	AC-CoRu-IW (A%)	AC-CoRe-IW (A%)	AC-Co-PR (A%)	AC-Co-US (A%)
C1s Scan								
carbodic carbon	282				7.0			
graphitic or aliphatic carbon	284–285	47.6	47.8	50.7	36.2	28.8	46.8	19.8
carbon in ethers, alcohols, phenols, amines, carbonyls, quinones, carboxyl or ester groups	286–291	12.6	13.0	21.9	14.7	9.8	11.8	7.9
π - π^* shake-up peaks	291–292	12.7	12.5	9.3	14.0	7.9	11.2	10.0
O1s Scan								
C=O groups	530	9.1	10.6	9.5	11.3	25.3	12.0	32.8
C-OH, C-O-C groups	532–533	10.0	8.4	2.9	9.0	14.7	9.1	11.0
chemisorbed O or water	534–536	3.6	2.4	0.9	3.5	4.2	2.9	5.9
Co2p Scan	779–782	4.0	4.8	0.9	4.6	6.0	4.8	13.8
N1s Scan	399	0.4	0.4	1.0	0.5	0.5	1.9	0.3

803 The peak area is calculated for each sample as atomic percent ratio

804

805

806

807 **Lahti *et al.* Figure captions**

808

809 Figure 1. Scheme for the preparation methods of cobalt catalysts on activated carbon support.

810

811

812

813

814

815

816

817

818

819

820

821

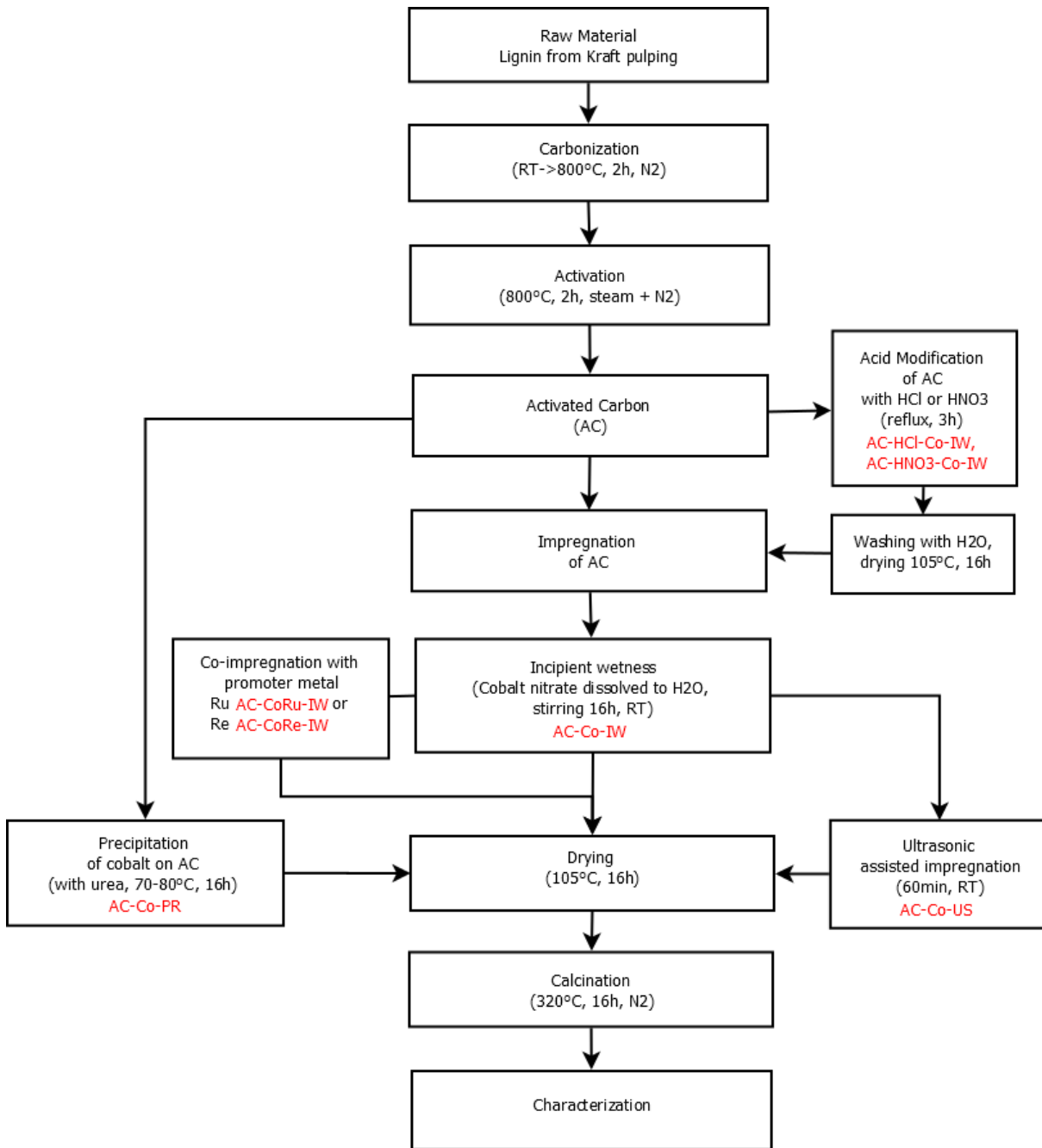
822

823

824

825

826



828

829

830

831

832 **Lahti *et al.* Figure captions**

833 Figure 2. FESEM (left) and TEM (right) images of catalyst AC-Co-IW.

834

835

836

837

838

839

840

841

842

843

844

845

846

847

848

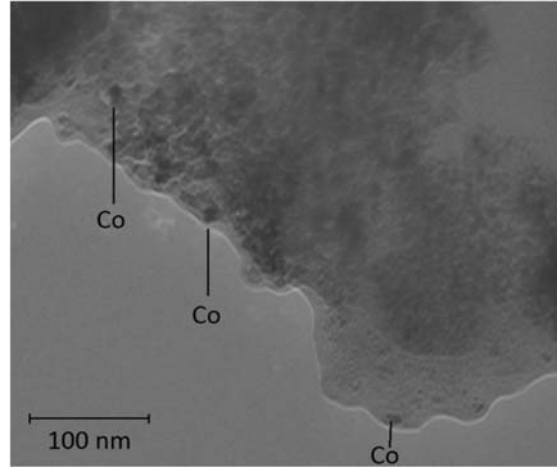
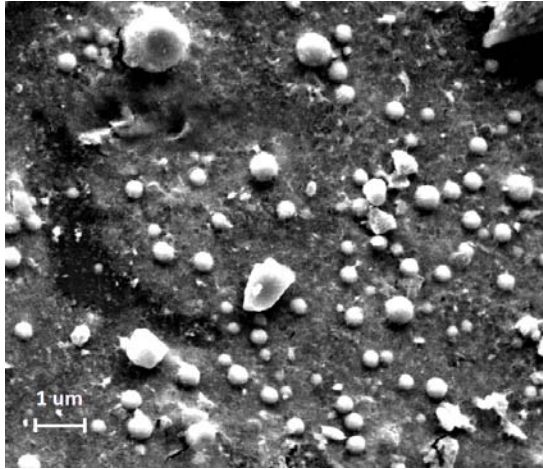
849

850

851

852 Lahti et al. Fig 2.

853



854

855

856

857

858

859

860

861

862

863

864

865

866 **Lahti et al. Figure captions**

867 Figure 3. SEM-EDS spectrum from catalyst AC-HNO₃-Co-IW.

868

869

870

871

872

873

874

875

876

877

878

879

880

881

882

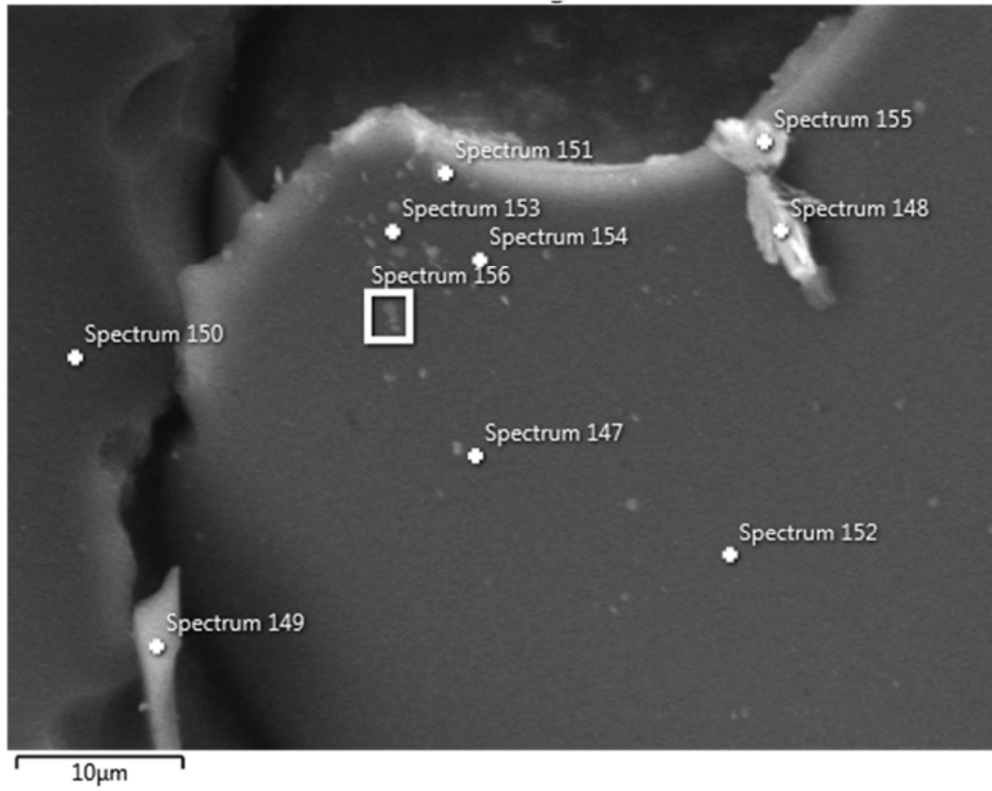
883

884

885

886 Lahti et al. Fig 3.

887



888

889

890

891

892

893

894

895

896

897

898 **Lahti *et al.* Figure captions**

899 Figure 4. XRD diffraction pattern of Co/AC-catalysts.

900

901

902

903

904

905

906

907

908

909

910

911

912

913

914

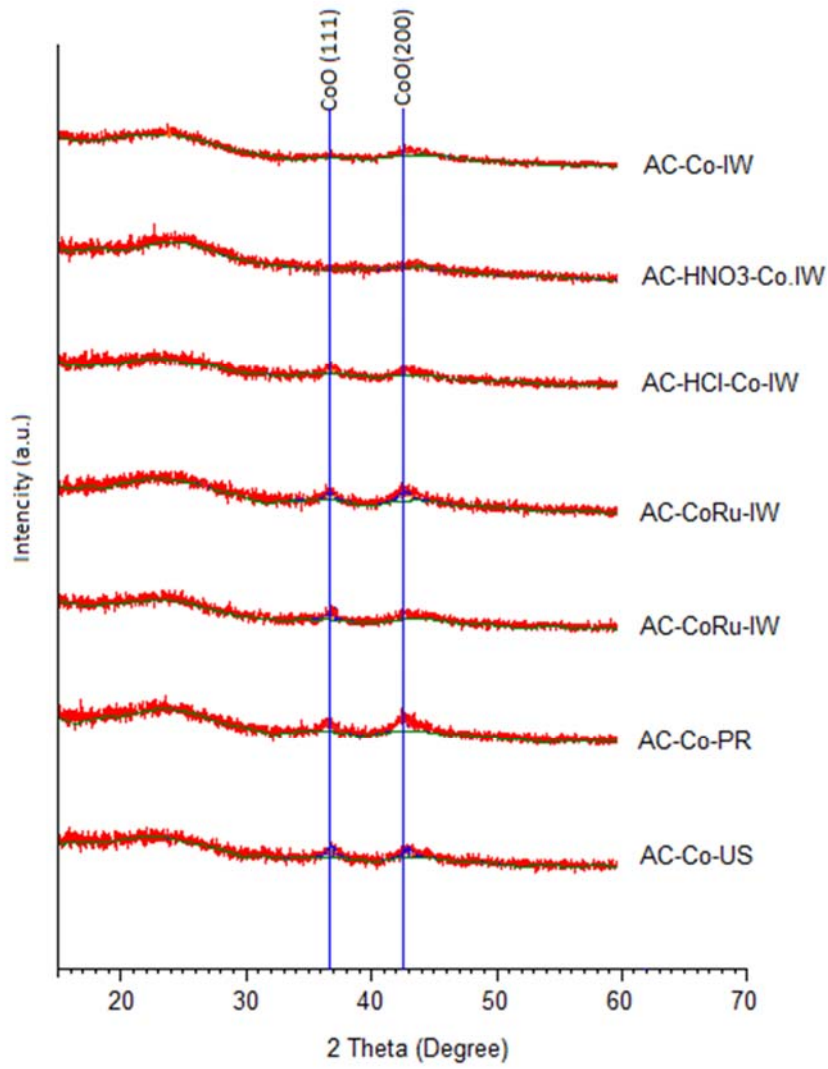
915

916

917

918 Lahti et al. Fig 4.

919



920

921

922

923

924

925

926 **Lahti *et al.* Figure captions**

927 Figure 5. H₂-TPR profiles for AC supported and SiO₂ supported Co-catalysts.

928

929

930

931

932

933

934

935

936

937

938

939

940

941

942

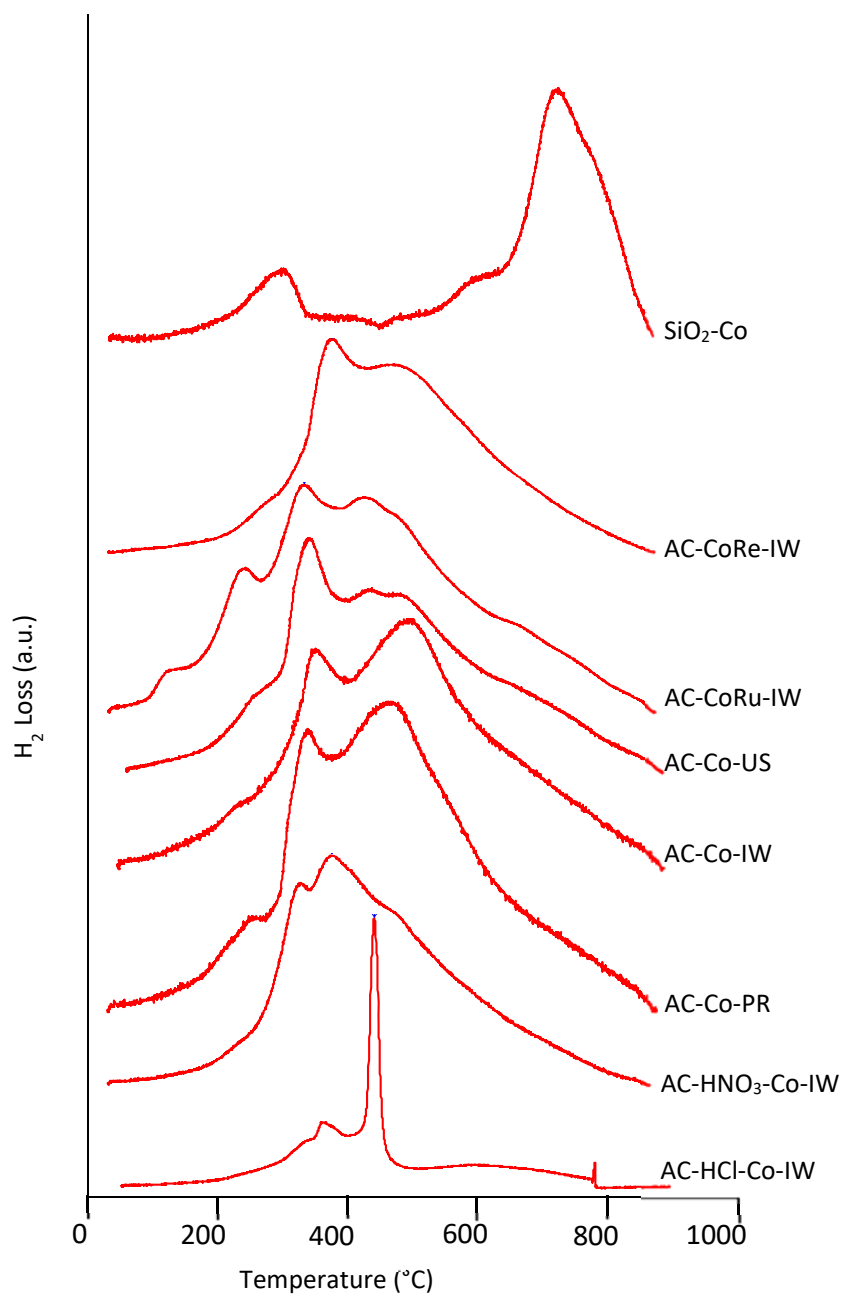
943

944

945

946 Lahti et al. Fig 5.

947



948

949

950

951 **Lahti *et al.* Figure captions**

952 Figure 6. DRIFTS spectrum for commercial AC, prepared AC and AC treated with HNO₃.

953

954

955

956

957

958

959

960

961

962

963

964

965

966

967

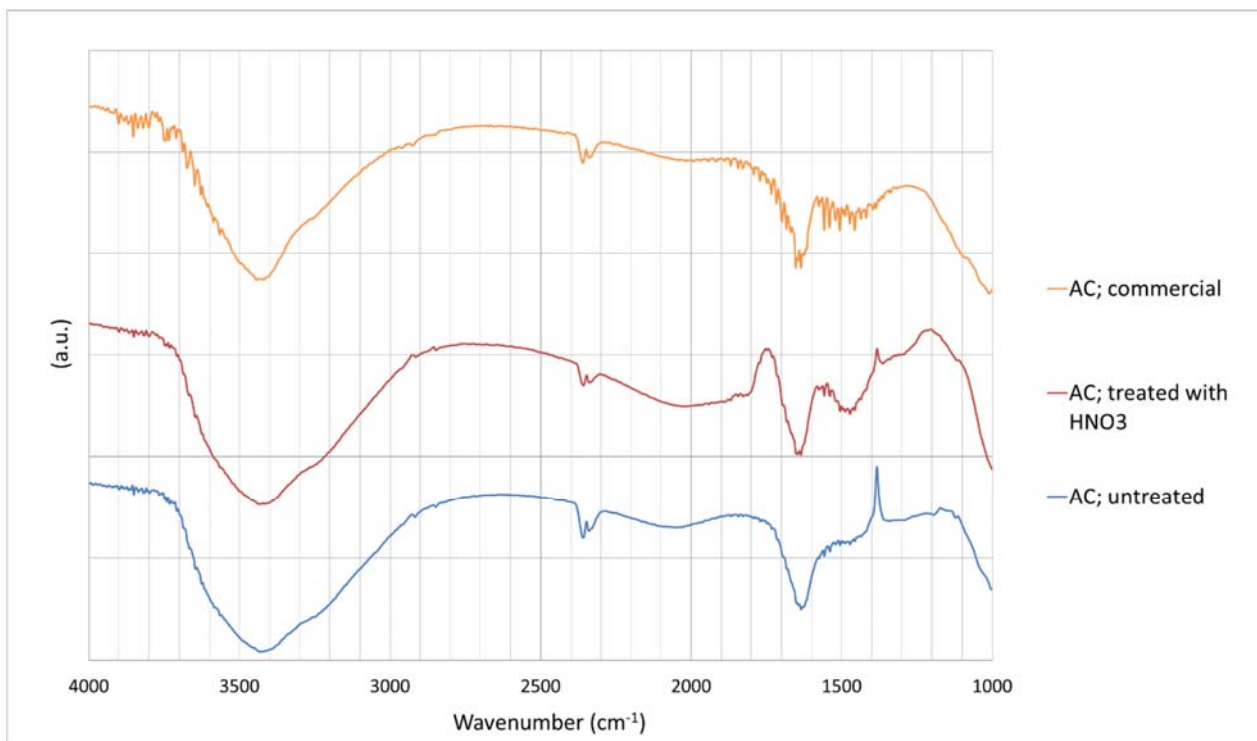
968

969

970

971 Lahti et al. Fig 6.

972



973

974

975

976

977

978

979

980

981

982

983 **Lahti et al. Figure captions**

984 Figure 7. High-resolution XPS spectrum of (a) C1s scans, (b) O1s scans, (c) Co2p -scans from Co/AC-catalysts.

985

986

987

988

989

990

991

992

993

994

995

996

997

998

999

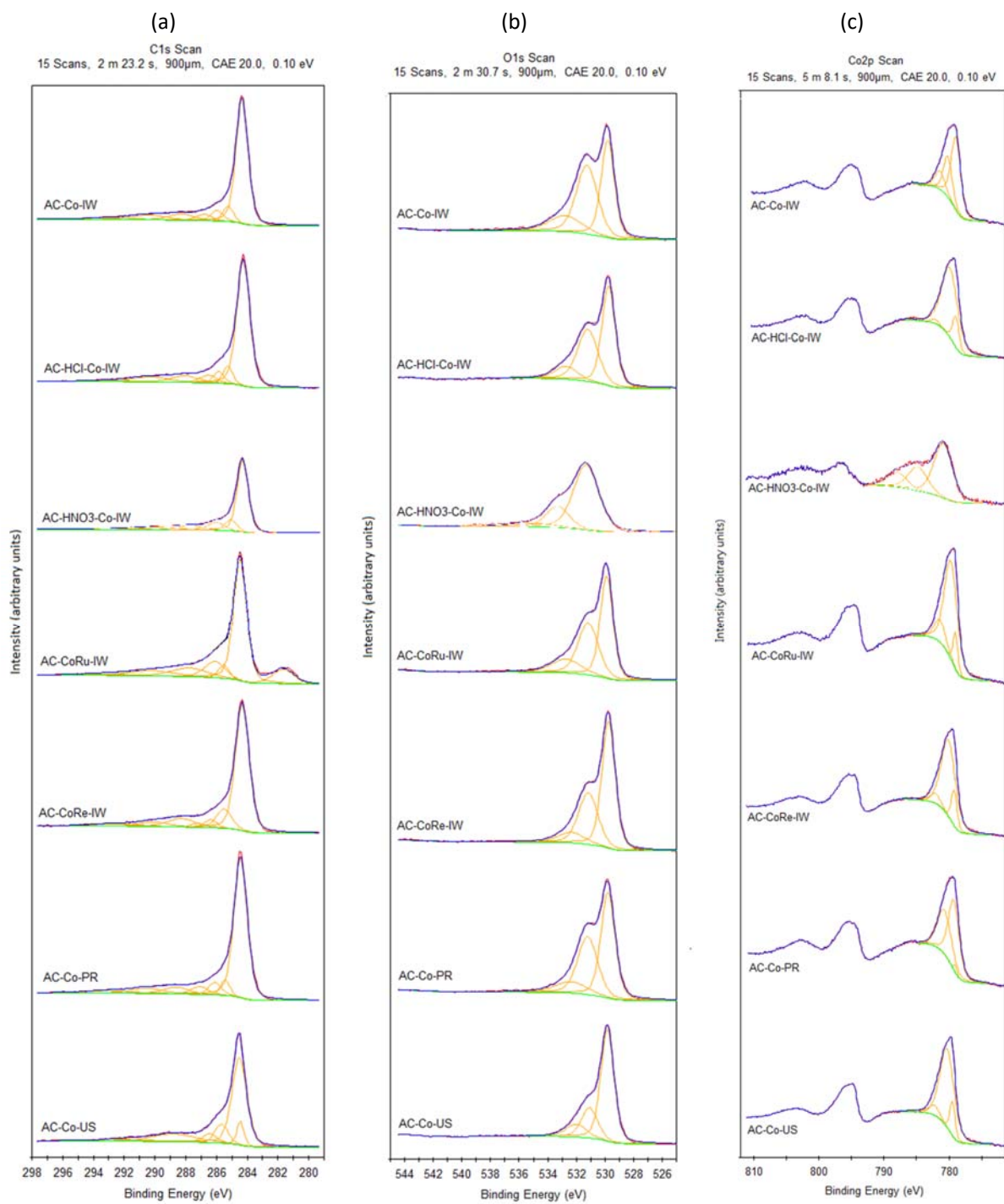
1000

1001

1002

1003 Lahti et al. Fig 7.

1004



1005

1006

1007 **Lahti *et al.* Figure captions**

1008 Figure 8. Functional groups on carbon surface from C1s, O1s, and Co2p -scans.

1009

1010

1011

1012

1013

1014

1015

1016

1017

1018

1019

1020

1021

1022

1023

1024

1025

1026

1027

1028

1029

1030

1031

1032

1033

1034

1035

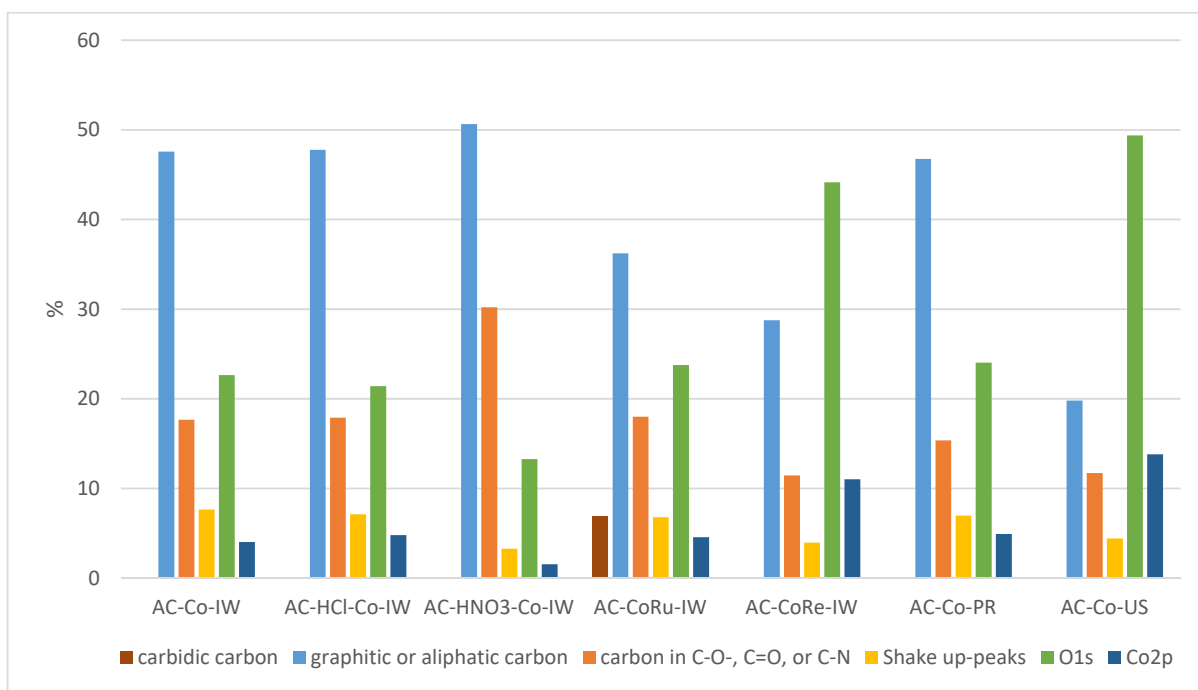
1036

1037

1038 Lahti et al. Fig 8.

1039

1040



1041

1042

1043

1044

1045

1046

1047

1048

1049

1050

1051 **Referees**

1052 Professor Edd Anders Blekkan, edd.a.blekkan@ntnu.no

1053 Professor Harry Bitter, j.h.bitter@uu.nl

1054 Kari Cook, kari@cookengineer.com

1055